JOURNAL OF Bio-X Research

RESEARCH ARTICLE

http://dx.doi.org/10.1097/JBR.0000000000000121

OPEN

In vivo detection of metabolic ^{2}H-incorporation upon ingestion of ^2H_2O

Kim Arnold[a,b], Xing Chen[c], Hui Zhang[d,e], Kapil Dev Singh[a,b], Zhihong Yin[c], Yao Yao[f], Tiangang Luan[f,g], Pablo Sinues[a,b,*], Xue Li[c,*]

Abstract

Objective: The aim of this work was to explore the feasibility of *in vivo* and non-invasive monitoring of deuterium/hydrogen (^{2}H/^{1}H) exchange at the metabolic level upon exposure to heavy water (^2H_2O).

Methods: The healthy female mice were randomly assigned to two groups after day 0 when both mice received standard drinking water. The treated mouse was fed with ^2H_2O (80%, v/v) and the control mouse fed with standard drinking water (H_2O) over next 13 days. Real-time mass spectrometric analysis of volatile metabolism emitted through breathing and the skin was performed on days 1, 2, 3, 10, 12, and 13. Animal experiment was approved by the Laboratory Animal Ethics Committee of Jinan University (approval No. 20161117163322) on October 29, 2021.

Results: We observed a replacement of ^{1}H by ^{2}H in 52 mass spectral features (60 ^{2}H/^{1}H isotopologue pairs) for the mouse fed with ^2H_2O, but not for the control mouse. These included pyruvic acid and lactic acid, lysine and methyl-lysine as well as short-chain fatty acids comprising acetic acid, propionic acid, butyric acid and valeric acid.

Conclusion: Secondary electrospray ionization-high resolution mass spectrometry allows monitoring *in vivo* ^{2}H-incorporation of metabolites in a non-invasive and real-time setup and opens new opportunities to use ^{2}H tracing to extend current metabolic studies, especially those with a focus on anaerobic glycolysis, lysine methylation and gut microbiome via monitoring of short-chain fatty acids.

Keywords: deuterium, isotopes, metabolomics, non-invasive, secondary electrospray ionization-high resolution mass spectrometry

Introduction

The elucidation of biochemical and metabolic pathways is the key to a deep understanding of biological systems. Stable isotopes such as deuterium (^{2}H) are powerful tools to achieve this endeavor. ^{2}H has been used as a tracer in various studies since the 1930s[1] because it offers several advantages over other isotopes: it is cheap, stable over long times, equilibrates quickly in body water and it can be delivered in a non-invasive way.[2] Furthermore, ^{2}H has been deployed as a metabolic tracer in combination with different mass spectrometric methods such as hydrogen (^{1}H)/^{2}H exchange (HDX) mass spectrometry (MS) to explore dynamic protein structure or protein interactions and to study fatty acid/lipid biosynthesis.[3–8] However, the availability of *in vivo*, non-invasive dynamic monitoring tools is still scarce. A recent work by Shi et al[9] showed the potential of combining heavy water (^2H_2O) with stimulated Raman scattering microscopy to image in *situ* metabolic activities in living organisms. In this work, we introduce a complementary method whereby we dynamically monitor the substitution of ^{1}H by ^{2}H in metabolites ultimately excreted via skin and/or breathing in mice upon drinking ^2H_2O.

Secondary electrospray ionization is an efficient ambient ionization method that, when combined with high-resolution mass spectrometry (SESI-HRMS), enables capturing fine isotopic structures. This makes it ideal for real-time observation of metabolic activity in living systems by monitoring the incorporation of isotopes upon introduction of labeled substrates (eg, metabolism of glucose by yeast).[10] Such information reflects changes in the intrinsic metabolome and helps for a better understanding of underlying metabolic processes, drug pharmacokinetics and disease-related alterations.[11,12] In this study we used an untargeted approach to investigate the capability of SESI-HRMS as a complementary technique to dynamically monitor metabolic ^{2}H-incorporation *in vivo* in a non-invasive and realtime manner.

Materials and methods

Animals

Two healthy female specific-pathogen-free C57BL/6 mice weighing 18 to 22 g were used in this study. Mice were

[a] University of Basel Children's Hospital (UKBB), Basel, [b] Department of Biomedical Engineering, University of Basel, Allschwil, Switzerland, [c] Institute of Mass Spectrometry and Atmospheric Environment, Jinan University, [d] School of Biomedical and Pharmaceutical Sciences, Guangdong University of Technology, [e] Metabolic Innovation Center, Zhongshan School of Medicine, Platform of Metabolomics, Center for Precision Medicine, [f] State Key Laboratory of Biocontrol, School of Life Sciences, Sun Yat-sen University, [g] Institute of Environmental and Ecological Engineering, Guangdong University of Technology, Guangzhou, Guangdong Province, China

[*] Corresponding authors: Pablo Sinues, University of Basel Children's Hospital (UKBB), Basel, Switzerland. E-mail: pablo.sinues@ukbb.ch; Xue Li, Institute of Mass Spectrometry and Atmospheric Environment, Jinan University, Guangzhou, Guangdong Province, China. E-mail: tamylee@jnu.edu.cn.

Journal of Bio-X Research (2022) 5:81–89

Received: 22 October 2021; Accepted: 17 February 2022

Published online xx month 2022

http://dx.doi.org/10.1097/JBR.0000000000000121

purchased from Guangdong Medical Laboratory Animal Center (Foshan, China) and housed under specific-pathogen-free conditions at 22 ± 2°C on a 12-hour light/dark cycle, and fed using standard mouse chow and water ad libitum. The mice were acclimatized for 1 week before the experiment began. Animal experiment was approved by the Laboratory Animal Ethics Committee of Jinan University (No. 20161117163322) on October 29, 2021 and conducted in strict accordance with international laws and National Institutes of Health (NIH) policies, including the Care and Use of Laboratory Animals (NIH publication no. 85-23, 1985, revised 1996).

SESI-HRMS analysis

On day 0 (D0), that is, 1 day before the treatment with ^2H_2O, both mice were fed with standard drinking water (H_2O) and a baseline measurement was acquired in both mice. Afterwards, mice were randomly divided into two groups. The treated group was fed with deuterium oxide (^2H_2O, 99.9 atom % ^2H, 80%, v/v, purchased from Merck, Darmstadt, Germany); the control group was fed with H_2O. Volatile species emitted by the mice were measured on days 1, 2, 3, 10, 12, and 13 for 20 minutes. SESI-HRMS analysis of mice's volatilome followed the procedures as reported previously.[13–15] The experimental setup is shown in Figure 1. Briefly, each mouse was placed in a polypropylene (PP) chamber in which a supply of medical grade air, free of volatile organic compounds (VOCs) at a steady flow rate of 1L/min, carried the emitted molecules into a lab-made SESI source. The carrier gas was produced by a zero-air generator (Beijing Anjiehua Co., Ltd., Beijing, China). The sample was ionized in the SESI source and directly analyzed by a high-resolution mass spectrometer (HRMS, Thermo Scientific Q-Exactive Orbitrap MS, Waltham, MA, USA) without sample pretreatment and chromatographic separation. MS measurements were performed in polarity-switch mode with a spray voltage of 2.5 kV; the ion transfer capillary temperature was set to 150°C. The mass range was *m/z* 50–750 and the resolution was set to 70,000. S-lens RF level was 50 and microscan was set to 1.

Sample size

This study was rather a "proof of principle." It is the very first time such hypothesis is tested and it was rather speculative to come up with any a priori hypothesis to base the power analysis. Our approach started with the minimum required number of animals, which is in fact $n=2$ (case and control) with an actual number of repeated measurements $n=12$. The analysis shown in this manuscript indicates that indeed $^2H/^1H$ ratio is up to around 2000 fold higher in the case mouse vs control (eg, Fig. 2F where ~0.3/0.000156 = 2000 as natural abundance of ^2H is 0.0156%). We therefore deem that the main claim made in this work is sufficiently justified.

Data analysis

Pre-processing. Data analysis was performed using MATLAB (version 2020b, MathWorks Inc., USA). Raw mass spectra files were converted to mzXML via msConvert (Proteowizard).[16] Positive and negative scans per file were filtered out. We then computed the average spectrum of 100 scans per file and the spectra were recalibrated using a polynomial fitting. After calibration, the mass accuracy across the entire mass range was within 2 ppm for both polarities (see an example of acetic acid in Additional Fig. 1, http://links.lww.com/JR9/A38). Subsequently, the spectra were centroided and binned using a Kernel density function, selecting its bandwidth to match the instrument

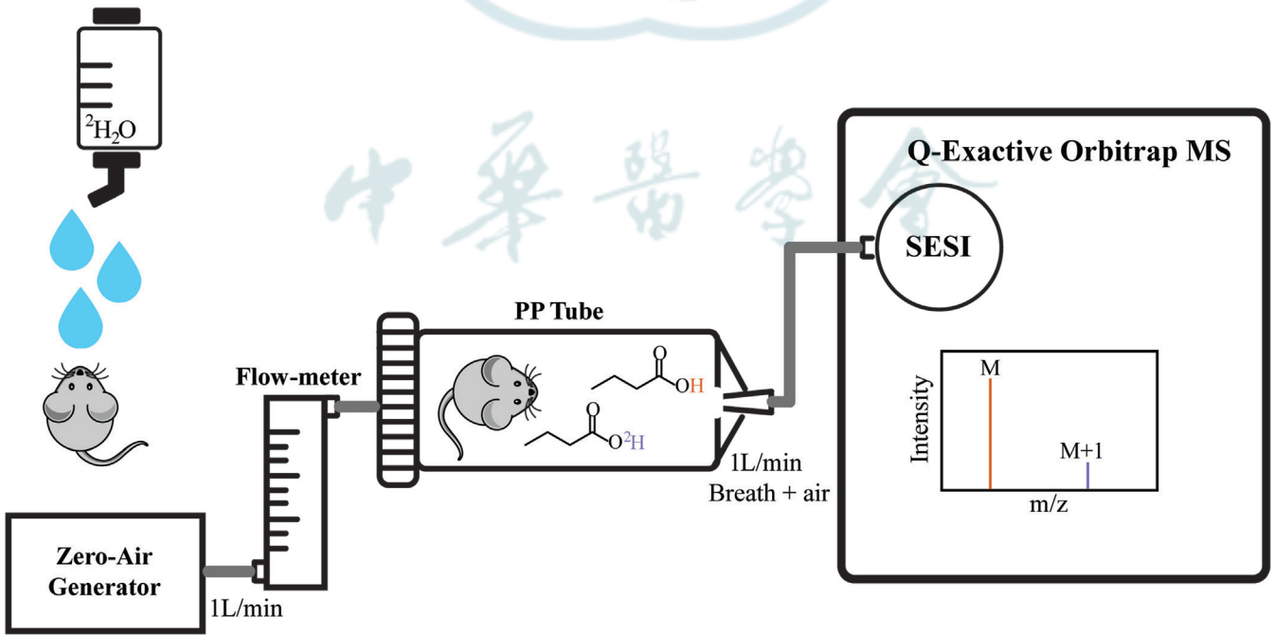

Figure 1. Schematic diagram of the experimental setup for real-time and *in vivo* monitoring of ^2H-incorporation. Mice were fed with ^2H_2O or H_2O respectively and placed in a polypropylene (PP) tube that was filled with 1L/min medical grade air produced by a zero-air generator and controlled by a flow-meter. Volatile species emitted by the mice were ionized in the SESI source and detected by a high-resolution mass spectrometer, enabling to resolve fine isotopic structures. ^2H=deuterium, ^2H_2O=heavy water, MS=mass spectrometer, SESI=secondary electrospray ionization.

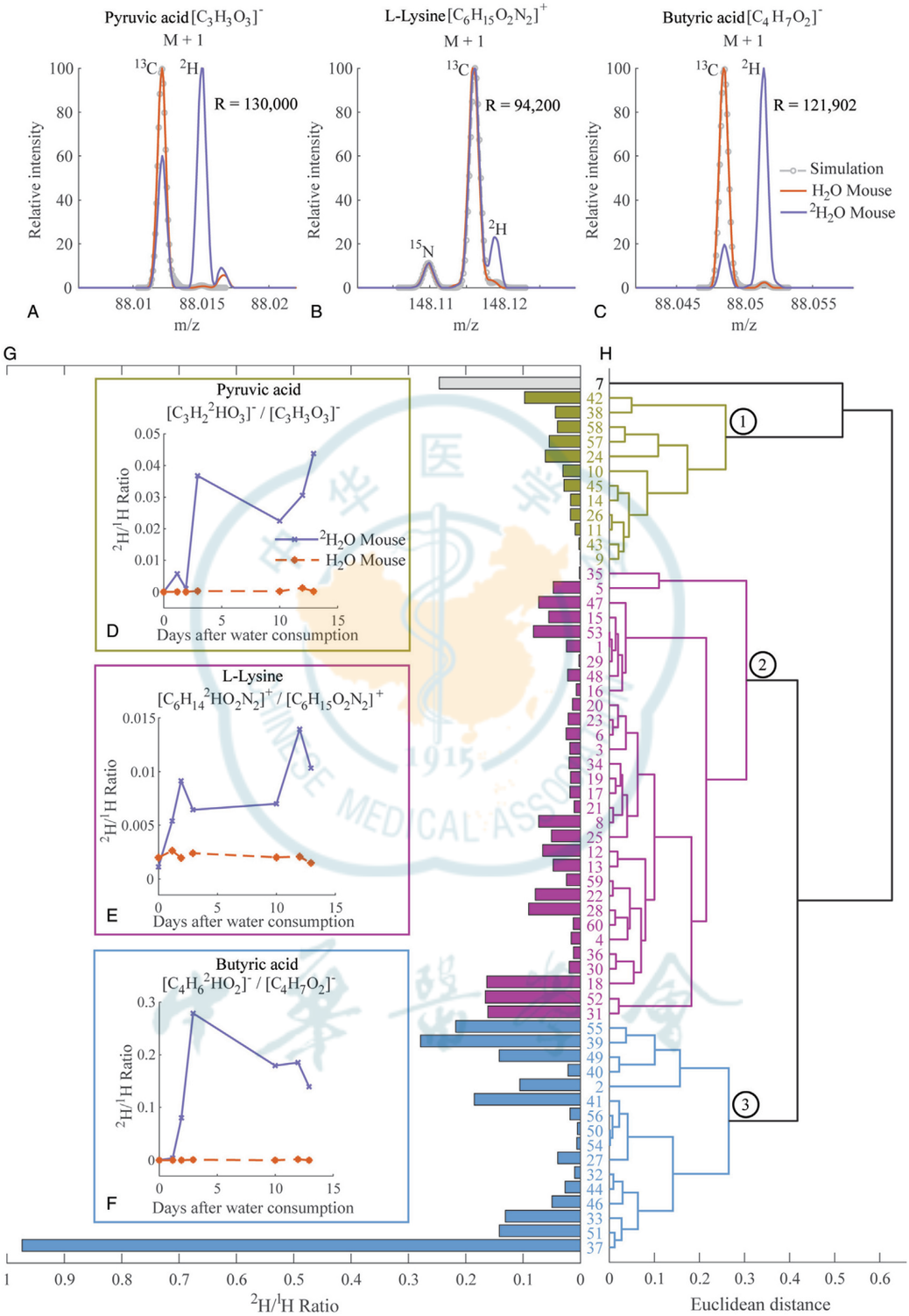

Figure 2. Mass spectra, $^{2}H/^{1}H$ ratio time traces, and clustergram of molecules showing relevant ^{2}H-incorporation. (A–C) M+1 mass spectra of pyruvic acid $[C_3H_3O_3]^-$ (A), L-Lysine $[C_6H_{15}O_2N_2]$+ (B), and butyric acid $[C_4H_7O_2]^-$ (C) acquired from $^{2}H_2O$ drinking mouse ($^{2}H_2O$ Mouse) and H_2O drinking mouse (H_2O Mouse) on the day when maximum $^{2}H/^{1}H$ ratio was reached in the mouse fed with $^{2}H_2O$. Isotopic simulation for the three ions is represented by the dash-dotted line. Peaks are normalized in respect to the most abundant peak present in that particular m/z region for the $^{2}H_2O$ mouse and H_2O mouse, respectively. Experimental resolution for each spectrum as well as ^{13}C and ^{2}H isotopic peaks are indicated. (D-F)$^{2}H/^{1}H$ ratio time traces of pyruvic acid [C3H3O3]$^-$ (D), L-Lysine $[C_6H_{15}O_2N_2]^+$ (E), and butyric acid $[C_4H_7O_2]^-$ (F) over 13 days of experiment observed in $^{2}H_2O$ mouse and H_2O mouse. (G) Bar chart representing maximum $^{2}H/^{1}H$ ratios obtained from $^{2}H_2O$ drinking mouse during the experiment. (H) Clustergram showing the hierarchical relationship between detected molecules and resulting in three clusters. Among others, cluster 1 contains pyruvic acid and lactic acid. Cluster 2 contains lysine and methyl-lysine. Both cluster 2 and cluster 3 contain SCFAs such as acetic acid, propionic acid and butyric acid. ^{1}H=hydrogen, ^{2}H=deuterium, $^{2}H_2O$=heavy water, SCFAs=short chain fatty acids.

resolution at each m/z. The final feature list was obtained by centroiding the resulting Kernel density function. The signal intensity for each feature was computed by summing the intensity of the peaks within their full width at half maximum. As a result, a data matrix of 14 samples (7 time points for mouse drinking H_2O and 7 time points for mouse drinking ^2H_2O) × 3476 features in positive mode and × 1407 features in negative mode was obtained.

Post-processing. In a first filtering step, the number of features was further reduced by considering only the cases were the signal intensity was greater than zero in at least four out of the seven data points measured for the mouse drinking ^2H_2O. Molecular formulae were assigned to the remaining 1350 positive and 1131 negative mode features based on the measured accurate mass within a tolerance of 2 ppm. Protonated (for positive mode features) and deprotonated species (for negative mode features) fulfilling "seven golden rules"[17] with only C, H, N and O were considered. $^2H/^1H$ isotopologue pairs were searched by identifying mass spectral features with a mass difference of $\Delta = n \times 1.0063u$ ($\pm$ 0.0005u), where $n = 1, 2 \ldots 10$ and u = unified atomic mass unit. The ratio of the signal intensities $^2H/^1H$ was computed for both mice at all the time points. Of the resulting $^2H/^1H$ time traces, only those showing an increasing trend in the mouse drinking ^2H_2O versus the control mouse were further considered (ie, 60 isotopologue pairs). Moreover, to explore similarities across the different kinetics of such ratio time traces, we conducted a hierarchical cluster analysis (average method; correlation distance). We then used the "lipids and non-lipids main chemical class" metabolite sets in MetaboAnalystR (version 3.0.3; https://www.metaboanalyst.ca)[18] to assign potential compound candidates to metabolites undergoing ^2H enrichment. Furthermore, compound hits were cross–referenced with HMDB (https://www.hmdb.ca) and KEGG (https://www.genome.jp/kegg) databases using "CrossReferencing" function of MetaboAnalystR.

Results

We identified 60 isotopologue $^2H/^1H$ pairs (26 in positive mode and 34 in negative mode) fulfilling the mass difference and increasing intensity criteria. Figure 2A shows the M+1 spectra of $[C_3H_3O_3]^-$ for the mice drinking H_2O and ^2H_2O at day 12, along with the simulated spectrum of $[C_3H_4O_3\text{-}H]^-$ at a resolution of 130,000, matching the experimental resolution at m/z 88. This ion has been previously identified as pyruvic acid.[19,20] Another example is shown in Figure 2B, whereby the most probable molecular formula at m/z 147.11268 was computed to be $[C_6H_{14}O_2N_2+H]^+$, which has been previously identified in human breath as lysine.[21]Figure 2C shows an additional example of butyric acid[22] in negative ion mode at m/z 88. The remaining M+1 mass spectra (zooming into ^{13}C and ^2H region) for which a molecular formula could be assigned are shown in Additional Figure 2 (http://links.lww.com/JR9/A38).

Once we identified the species undergoing a relevant incorporation of ^2H, we studied their evolution during the course of the experiment. Figure 2D–F shows the three representative $^2H/^1H$ ratio time traces of the mass spectra presented in Figure 2A–C for the two mice (ie, ^2H_2O and H_2O drinking mice) over 13 days. A difference among the temporal profiles of the traces is clearly visible. For example, pyruvic acid spiked to nearly 4% on day 3 and then remained in that region until the end of the experiment (Fig. 2D). Lysine steadily increased until ~1% on day 3 and peaked on day 12 at nearly 1.5% (Fig. 2E). In contrast, butyric acid remained at the natural abundance level until day one and then raised on days 2 and 3 up to nearly 30%. Afterward, it declined during the subsequent days down to around 13% (Fig. 2F). Additional Figures 3 and 4 (http://links.lww.com/JR9/A38) present the rest of the explored time traces. Figure 2G shows a bar plot indicating the maximum $^2H/^1H$ ratio observed for each of the 60 detected pairs of ions, which in most cases occurred on day 12 after first exposure to ^2H_2O.

To gain further insights into such different temporal patterns, we subjected the ratio time traces to hierarchical cluster analysis as illustrated in Figure 2H which reveals three major groups. Cluster 1 contains pyruvic acid (#38) in close relation to lactic acid (#42). Cluster 2 contains lysine (#20), which interestingly clusters together with m/z 161.1284 (#23) and fits with the molecular formula of methyl-lysine (Table 1). In this cluster and cluster 3 we found the three short chain fatty acids (SCFAs) (ie, acetic acid, propionic acid, and butyric acid). Table 1 lists the 60 isotopologue $^2H/^1H$ pairs identified during this study. Among the 52 discovered mass spectral features undergoing ^2H enrichment, 21 instances had a hit attributed by cross-referencing HMDB and KEGG databases.

Discussion

In this study we showed for the first time that SESI-HRMS is a suitable tool to detect metabolic ^2H-incorporation *in vivo* and in real-time. The technique has the required sensitivity (ie, part-pertrillion range[23]) to enable the detection of species emitted under physiological conditions without any sample preconcentration. At the same time, it renders the required mass resolution to enable the separation of fine isotopic structures. The perfect match between the simulated spectra and the experimental ones from the mouse drinking H_2O obtained for pyruvic acid, lysine and butyric acid (Fig. 2A-C) provides confidence on the calibration procedure (within 2 ppm) and on the possibility to resolve ^{13}C and ^2H isotopic peaks. Even the ^2H peak of lysine (Fig. 2B) is partially resolved from the latter at a resolution of ~94,000. The perfect overlap in terms of both – m/z and relative intensity domains – provides in addition further reassurance on the molecular formula assignments made for all ions. The striking relative increase of the ^2H peak for the mouse drinking heavy water suggests that non-invasively monitoring the *in vivo* incorporation of ^2H in metabolites over an extended period of time is feasible.

As expected, the temporal profiles of the $^2H/^1H$ ratios remained constant over the days for the control mouse, close to zero (Fig. 2D–F). In contrast, for the mouse drinking heavy water a steady increase in ratio was observed after day 0 (ie, baseline). Besides the different dynamics observed for the $^2H/^1H$ trajectories (Fig. 2D–F), butyric acid was interestingly one of the four examples of SCFAs that we found to undergo a detectable exchange of two (out of its seven) hydrogens (Additional Fig. 3, http://links.lww.com/JR9/A38). The kinetic profile of $^2H_2/^1H$ for butyric acid resembled very much the one for $^2H/^1H$; however, its maximum ratio was around ten times lower (ie, ~3% instead of ~30% at day 3). We found a similar behavior for all SCFAs as well as for lactic acid (Additional Fig. 3, http://links.lww.com/JR9/A38). However, for the latter, the ratio trended towards a clear increase as the days passed by (ie, accumulation effect). Such disparity in the $^2H/^1H$ ratio scale and kinetics suggests different mechanisms for the ultimate incorporation of

Table 1

Isotopologue pairs identified to show ^{2}H-incorporation.

m/z ^{1}H	m/z $^{2}H_n$	n (^{2}H)	Molecular formula (M)*	Adduct	Absolute mass error (ppm)	Compound hits#	HMDB ID	KEGG ID	Cluster ID†	Cluster ref‡
89.0710	93.0962	4	$C_3H_8N_2O$	[M + H] +	0.690	Dimethylurea	HMDB0029198	C16364	7	1
89.0244	90.0307	1	$C_3H_6O_3$	[M – H] –	0.191	Hydroxypropionic acid (Lactic acid) / Dihydroxyacetone / Glyceraldehyde	HMDB0000700 / HMDB0001882 / HMDB0001051	C01013 / C00184 / C02154	42	1
87.0088	88.015	1	$C_3H_4O_3$	[M – H] –	0.373	2-hydroxyacrylic Acid / 3-Hydroxypro-penoate / Malonic semialdehyde / Pyruvic acid	NA / NA / HMDB0011111 / HMDB0000243	NA / NA / C00222 / C00022	38	1
122.0221	123.0283	1	NA	[M + H] +	NA	NA	NA	NA	58	1
121.0659	122.0721	1	$C_8H_{10}O$	[M– H] –	0.098	2,4,6-Octatrienal / 1-Phenylethanol /2-Pheny-lethanol / 4-Ethylphenol	NA / HMDB0032619 /HMDB0033944 /HMDB0029306	NA / C07112 /C05853 /C13637	57	1
178.1437	182.169	4	$C_8H_{19}NO_3$	[M + H] +	0.392	NA	NA	NA	24	1
92.0899	93.0962	1	NA	[M + H] +	NA	NA	NA	NA	10	1
90.0277	91.0341	1	NA	[M – H] –	NA	NA	NA	NA	45	1
124.0968	125.1032	1	$C_4H_{13}NO_3$	[M + H] +	0.158	NA	NA	NA	14	1
181.1626	182.169	1	NA	[M + H] +	NA	NA	NA	NA	26	1
92.0929	93.0992	1	NA	[M + H] +	NA	NA	NA	NA	11	1
89.0244	91.037	2	$C_3H_6O_3$	[M – H] –	0.191	Hydroxypropionic acid (Lactic acid)/ Dihydroxyacetone / Glyceraldehyde	HMDB0000700 / HMDB0001882 / HMDB0001051	C01013 / C00184 / C02154	43	1
91.0866	93.0992	2	$C_3H_{10}N_2O$	[M + H] +	0.120	NA	NA	NA	9	1
77.9958	79.0022	1	NA	[M – H] –	NA	NA	NA	NA	35	2
78.0662	79.0724	1	NA	[M + H] +	NA	NA	NA	NA	5	2
92.0227	93.029	1	NA	[M – H] –	NA	NA	NA	NA	47	2
127.1116	129.1243	2	$C_8H_{14}O$	[M + H] +	1.120	2-Octenal / Sulcatone	HMDB0030961 / HMDB0035915	NA / C07287	15	2
117.0557	118.0619	1	$C_5H_{10}O_3$	[M – H] –	0.146	2-Ethylhydracrylic acid / 2-Hydroxy-2-methylbutyric acid / 2-Hydroxy-3-methyl-butyric acid / 2-Hydroxyvale-ric acid / 2-Methyl-3-hydroxybutyric acid / 2-Methyl-3-hydroxypropanoic acid / 3-Hydroxy-2-methyl-[R-(R,S)]-butanoic acid / 3-Hydroxyisovaleric acid / 3-Hydroxyvaleric acid / 5-Hydroxyvaleric acid / Erythronilic acid / Methyl-2-hydoxyisobutyric acid	HMDB0000396 / HMDB0001987 / HMDB0000407 / HMDB0001863 / HMDB0000354 / HMDB0126088 / HMDB0000351 / HMDB0000754 / HMDB0000531 / HMDB0061927 / HMDB0000642 / NA	NA / NA / NA / NA / NA / NA / NA / C20827 / NA / C02804 / NA / NA	53	2

Table 1
(continued).

m/z ^{1}H	m/z ^2H_n	n (^{2}H)	Molecular formula (M)*	Adduct	Absolute mass error (ppm)	Compound hits#	HMDB ID	KEGG ID	Cluster ID†	Cluster ref‡
60.0444	61.0506	1	C_2H_5NO	[M + H] +	0.166	Acetamide / N-Methylformamide	HMDB0031645 / HMDB0001122	C06244 / C11489	1	2
59.0139	61.0263	2	$C_2H_4O_2$	[M − H] −	0.790	Acetic acid / Glycolaldehyde	HMDB0000042 / HMDB0003344	C00033 / C00266	29	2
93.9908	94.9971	1	NA	[M − H] −	NA	NA	NA	NA	48	2
127.1116	130.1308	3	$C_8H_{14}O$	[M + H] +	1.120	2-Octenal / Sulcatone	HMDB0030961 /	NA / C07287	16	2
147.1127	148.1187	1	$C_6H_{14}N_2O_2$	[M + H] +	0.710	L-Lysine	HMDB0035915 HMDB0000182	C00047	20	2
161.1284	162.1349	1	$C_7H_{16}N_2O_2$	[M + H] +	0.336	Isoputreanine / N(2)-Methyl-lysine / N (6)-Methyllysine	HMDB0006009 / NA / HMDB0002038	NA / NA / C02728	23	2
88.0757	89.0819	1	C_4H_9NO	[M + H] +	0.113	2-Methylpropanal oxime	HMDB0031243	C03219	6	2
74.0601	75.0663	1	C_3H_7NO	[M + H] +	0.819	3-Aminopropionaldehyde / Aminoacetone / N,N-Dimethylformamide	HMDB0001106 / HMDB0002134 / HMDB0001888	C05665 / C01888 / C03134	32	
76.9880	77.9943	1	NA	[M − H] −	NA	NA	NA	NA	34	2
136.1119	137.118	1	$C_9H_{13}N$	[M + H] +	1.300	NA	NA	NA	19	2
128.1433	129.1493	1	$C_8H_{17}N$	[M + H] +	0.595	(S)-2-Propylpiperidine	HMDB0030285	C06523	17	2
148.1160	149.1223	1	NA	[M + H] +	NA	NA	NA	NA	21	2
91.0866	92.0929	1	$C_3H_{10}N_2O$	[M + H] +	0.120	NA	NA	NA	8	2
180.1593	181.1659	1	$C_8H_{21}NO_3$	[M + H] +	0.667	NA	NA	NA	25	2
105.1022	106.1084	1	$C_4H_{12}N_2O$	[M + H] +	0.377	NA	NA	NA	12	2
119.1178	120.124	1	$C_5H_{14}N_2O$	[M + H] +	0.755	NA	NA	NA	13	2
123.9888	124.9951	1	NA	[M − H] −	NA	NA	NA	NA	59	2
152.1281	153.1343	1	$C_6H_{17}O_3N$	[M + H] +	0.128	NA	NA	NA	22	2
59.0139	60.0201	1	$C_2H_4O_2$	[M − H] −	0.790	Acetic acid / Glycolaldehyde	HMDB0000042 / HMDB0003344	C00033 / C00266	28	2
124.0377	125.0439	1	NA	[M − H] −	NA	NA	NA	NA	60	2
75.0634	76.0696	1	NA	[M + H] +	NA	NA	NA	NA	4	2
78.9911	79.9974	1	NA	[M + H] +	NA	NA	NA	NA	36	2
60.9931	61.9994	1	CH_2O_3	[M − H] −	0.294	Carbonic acid	HMDB0003538	C01353	30	2
134.0923	135.0984	1	$C_4H_{11}N_3O_2$	[M + H] +	0.772	NA	NA	NA	18	2
106.0272	107.0334	1	NA	[M − H] −		NA	NA	NA	52	2
73.0295	74.0358	1	$C_3H_6O_2$	[M − H] −	0.035	Propionic acid / 3-Hydroxy-propanal / Hydroxyacetone / Lactaldehyde	HMDB0000237 / HMDB0003453 / HMDB0006961 / HMDB0003052	C00163 / C00969 / C05235 / C00424	31	2
120.0428	121.049	1	NA	[M − H] −	NA	NA	NA	NA	55	3
87.0452	88.0515	1	$C_4H_8O_2$	[M − H] −	0.538	(R)-Acetoin / 3R-Hydroxybu-tan-2-one / Butyric acid / Isobutyric acid / Ethyl acet-ate	HMDB0003243 / NA / HMDB0000039 / HMDB0001873 / HMDB0031217	C00466 / NA / C00246 / C02632 / C00849	39	3
101.0608	102.0671	1	$C_5H_{10}O_2$	[M − H] −	0.026	Isovaleric acid / Valeric acid	HMDB0000718 / HMDB0000892	C08262 / C00803	49	3
87.0452	89.0577	2	$C_4H_8O_2$	[M − H] −	0.538	(R)-Acetoin / 3R-Hydroxybu-tan-2-one / Butyric acid /	HMDB0003243 / NA / HMDB0000039 /	C00466 / NA / C00246 / C02632 / C00849	40	3

Table 1

(continued).

m/z ^{1}H	m/z ^2H_n	n (^{2}H)	Molecular formula (M)*	Adduct	Absolute mass error (ppm)	Compound hits#	HMDB ID	KEGG ID	Cluster ID†	Cluster ref‡
						Isobutyric acid / Ethyl acetate	HMDB0001873 / HMDB0031217			
61.0396	62.0459	1	CH_4N_2O	[M + H] +	0.635	Urea	HMDB0000294	C00086	2	3
88.0485	89.0548	1	NA	[M – H] –	NA	NA	NA	NA	41	3
120.0428	122.0554	2	NA	[M – H] –	NA	NA	NA	NA	56	3
101.0608	103.0734	2	$C_5H_{10}O_2$	[M – H] –	0.026	Isovaleric acid / Valeric acid	HMDB0000718 / HMDB0000892	C08262 / C00803	50	3
118.0272	122.0524	4	NA	[M – H] –	NA	NA	NA	NA	54	3
57.0347	58.0409	1	C_3H_6O	[M– H] –	1.930	Acetone / Propanal	HMDB0001659 / HMDB0003366	C00207 / C00479	27	3
73.0295	75.0421	2	$C_3H_6O_2$	[M – H] –	0.035	Propionic acid / 3-Hydroxy-propanal / Hydroxyacetone / Lactaldehyde	HMDB0000237 / HMDB0003453 / HMDB0006961 / HMDB0003052	C00163 / C00969 / C05235 / C00424	32	3
89.9959	91.0021	1	NA	[M – H] –	NA	NA	NA	NA	44	3
92.0115	93.0178	1	NA	[M – H] –	NA	NA	NA	NA	46	3
74.0329	75.0392	1	NA	[M – H] –	NA	NA	NA	NA	33	3
104.0115	105.0177	1	NA	[M – H] –	NA	NA	NA	NA	51	3
85.0295	89.0548	4	$C_4H_6O_2$	[M – H] –	0.030	Butenoic acid / Diacetyl / Gamma-Butyrolactone / But-2-yne-1,4-diol / Oxolan-3-one	HMDB0010720 / HMDB0003407 / HMDB0000549 / NA / HMDB0002523	C01771 / C00741 / C01770 / NA / NA	37	3

* Formula based on accurate mass only (no isotopic pattern matching performed except for those molecules presented in Figure 2A-C). #Hits based on MetaboAnalystR (version 3.0.3) using "lipids and non-lipids main chemical class" metabolite sets. †ID in the clustergram ordered accordingly to Figure 2H from top to bottom. ‡Clusters of ions which are correlating with each other.^{1}H = Hydrogen, ^{2}H = deuterium, NA=not available.

^2H in the detected metabolites. For example, the maximum $^2H/^1H$ ratio was found to be nearly one for $C_4H_2{}^2H_4O_2/C_4H_6O_2$ (#37 in Fig. 2G). However, this was an outlier as the majority of the identified $^2H_n/H$ ratios corresponded to n=1 and the median ratio was in the order of 3% (median = 0.0296; interquartile range = 0.0631). There are mainly two mechanisms explaining the occurrence of $^2H/^1H$ exchange and therefore the different resulting kinetics: enzymatic irreversible exchange or non-enzymatic reversible exchange. In the former, ^2H_2O forms N-^2H, O-^2H and S-^2H bonds which occur faster and more often because $^2H/^1H$ exchange is more prominent when the hydrogen is bound to a heteroatom as a consequence of the intrinsic electronegativity provided by the free electron pair whereas in an enzymatic exchange ^2H_2O forms C-^2H bonds which is slower and dependent on the number of enzymes available and produced by the organism.[9,24–26] Whilst all the molecular formulae identified in this study contain either O and/or N-atoms, it is unclear at this point whether the observed ^2H-incorporations correspond enzymatic, non-enzymatic or both types of reactions.

Cluster analysis of the $^2H/^1H$ time traces revealed similarities in the temporal profiles of pyruvic acid and lactic acid with an increasing trend over the course of the days (cluster 1, Fig. 2H). Such phenomena can be explained by anaerobic glycolysis in red blood cells, muscle cells or gut microbiome, whereby glucose produces pyruvate, which is then converted to lactate when supply of oxygen is limited.[27,28] Clusters 2 and 3 revealed the presence of SCFAs which are the main products of gut microbiome activity and their importance in modulating other metabolic, endocrine and immune functions is becoming increasingly evident.[29]

Limitations

The proof-of-principle study had the following limitations: i) The sample size of n = 2 mice was admittedly small; ii) there was no control when and how much water the mice ingested; iii) the mass spectrometer could have been operated with an even higher resolution; and iv) the identification of the relevant compounds remained putative since no MS/MS experiments were performed to confirm the compound identity.

Conclusion

SESI-HRMS allows real-time, *in vivo* and non-invasive tracing of the incorporation of ^2H in metabolites, opening new possibilities for metabolomics studies.

Acknowledgements

The authors thank Philipp Keller (Institute of Microbiology, Department of Biology, ETH Zurich Switzerland) for his advice in regard to data analysis aspects.

Author contributions

XC, ZY, and YY contributed to mouse experiments. KA, KDS, and PS contributed to data analysis, data interpretation and manuscript drafting and writing. TL, HZ, and XL contributed to the study design, data pre-processing and manuscript editing and review. All authors approved the final version of the manuscript.

Financial support

This work was supported by a grant from Fondation Botnar (Switzerland) and the Swiss National Science Foundation (Nos. 320030_173168 and PCEGP3_181300; to PS), the National Natural Science Foundation of China (No. 22122603; to XL), Guangdong Special Support Program (No. 2019BT02Z546; to XL), Guangdong Natural Science Foundation (Nos. 2018A030313790 and 2017GC010648; to HZ). The funders did not participate in data collection and analysis, article writing or submission.

Institutional review board statement

Animal experiment was approved by the Laboratory Animal Ethics Committee of Jinan University (approval No. 20161117163322) on October 29, 2021.

Conflicts of interest

PS is cofounder of Deep Breath Intelligence AG (Switzerland), which develops breath-based diagnostic tools.

References

[1] Schoenheimer R, Rittenberg D. Deuterium as an indicator in the study of intermediary metabolism. Science 1935;82:156–157.
[2] Miyagi M, Kasumov T. Monitoring the synthesis of biomolecules using mass spectrometry. Philos Trans A Math Phys Eng Sci 2016;374:20150378.
[3] Vadas O, Jenkins ML, Dornan GL, et al. Using hydrogen-deuterium exchange mass spectrometry to examine protein-membrane interactions. Methods Enzymol 2017;583:143–172.
[4] Lee WN, Bassilian S, Ajie HO, et al. In vivo measurement of fatty acids and cholesterol synthesis using D2O and mass isotopomer analysis. Am J Physiol 1994;266:E699–E708.
[5] Zhang Z, Vachet RW. Kinetics of protein complex dissociation studied by hydrogen/deuterium exchange and mass spectrometry. Anal Chem 2015;87:11777–11783.
[6] Miller BF, Reid JJ, Price JC, et al. CORP: The use of deuterated water for the measurement of protein synthesis. J Appl Physiol 19852020;128:1163–1176.
[7] Engen JR, Botzanowski T, Peterle D, et al. Developments in hydrogen/deuterium exchange mass spectrometry. Anal Chem 2021;93:567–582.
[8] Fu X, Deja S, Fletcher JA, et al. Measurement of lipogenic flux by deuterium resolved mass spectrometry. Nat Commun 2021;12:3756.
[9] Shi L, Zheng C, Shen Y, et al. Optical imaging of metabolic dynamics in animals. Nat Commun 2018;9:2995.
[10] Tejero Rioseras A, Garcia Gomez D, Ebert BE, et al. Comprehensive realtime analysis of the yeast volatilome. Sci Rep 2017;7:14236.
[11] Singh KD, Osswald M, Ziesenitz VC, et al. Personalised therapeutic management of epileptic patients guided by pathway-driven breath metabolomics. Commun Med 2021;1:21.
[12] Shirasu M, Touhara K. The scent of disease: volatile organic compounds of the human body related to disease and disorder. J Biochem 2011;150:257–266.
[13] Yin Z, Huang W, Singh KD, et al. In vivo monitoring of volatile metabolic trajectories enables rapid diagnosis of influenza A infection. Chem Commun (Camb) 2021;57:4791–4794.
[14] Chen X, Zhang K, Yin Z, et al. Online real-time monitoring of exhaled breath particles reveals unnoticed transport of nonvolatile drugs from blood to breath. Anal Chem 2021;93:5005–5008.
[15] Li X, Martinez-Lozano Sinues P, Dallmann R, et al. Drug pharmacokinetics determined by real-time analysis of mouse breath. Angew Chem Int Ed Engl 2015;54:7815–7818.
[16] Kessner D, Chambers M, Burke R, et al. ProteoWizard: open source software for rapid proteomics tools development. Bioinformatics 2008;24:2534–2536.
[17] Kind T, Fiehn O. Seven Golden Rules for heuristic filtering of molecular formulas obtained by accurate mass spectrometry. BMC Bioinformatics 2007;8:105.

[18] Chong J, Xia J. MetaboAnalystR: an R package for flexible and reproducible analysis of metabolomics data. Bioinformatics 2018;34:4313–4314.
[19] Martínez-Lozano P, de la Mora JF. On-line detection of human skin vapors. J Am Soc Mass Spectrom 2009;20:1060–1063.
[20] Martínez-Lozano P, Fernández de la Mora J. Direct analysis of fatty acid vapors in breath by electrospray ionization and atmospheric pressure ionization-mass spectrometry. Anal Chem 2008;80:8210–8215.
[21] Garcia-Gomez D, Gaisl T, Bregy L, et al. Real-time quantification of amino acids in the exhalome by secondary electrospray ionization-mass spectrometry: a proof-of-principle study. Clin Chem 2016;62:1230–1237.
[22] Adam ME, Fehervari M, Boshier PR, et al. Mass-spectrometry analysis of mixed-breath, isolated-bronchial-breath, and gastric-endoluminal-air volatile fatty acids in esophagogastric cancer. Anal Chem 2019;91:3740–3746.
[23] Martínez-Lozano P, Rus J, Fernández de la Mora G, et al. Secondary electrospray ionization (SESI) of ambient vapors for explosive detection at concentrations below parts per trillion. J Am Soc Mass Spectrom 2009;20:287–294.
[24] Kostyukevich Y, Acter T, Zherebker A, et al. Hydrogen/deuterium exchange in mass spectrometry. Mass Spectrom Rev 2018;37:811–853.
[25] Grocholska P, Bachor R. Trends in the hydrogen-deuterium exchange at the carbon centers. preparation of internal standards for quantitative analysis by LC-MS. Molecules 2021;26:2989.
[26] Englander SW, Sosnick TR, Englander JJ, et al. Mechanisms and uses of hydrogen exchange. Curr Opin Struct Biol 1996;6:18–23.
[27] Bender DA, Caballero B. GLUCOSE j Function and Metabolism. Encyclopedia of Food Sciences and Nutrition. 7th ed.2003;Academic Press, 2904-2911.
[28] Pessione E. Lactic acid bacteria contribution to gut microbiota complexity: lights and shadows. Front Cell Infect Microbiol 2012;2:86.
[29] Dalile B, Van Oudenhove L, Vervliet B, et al. The role of short-chain fatty acids in microbiota-gut-brain communication. Nat Rev Gastroenterol Hepatol 2019;16:461–478.